Journal of Power Sources 241 (2013) 696–702

Contents lists available at SciVerse ScienceDirect

Journal of Power Sources

journal homepage: www.elsevier.com/locate/jpowsour

PdRu/C catalysts for ethanol oxidation in anion-exchange membrane direct ethanol fuel cells

Liang Ma [a], Hui He [b], Andrew Hsu [b], Rongrong Chen [a,*]

[a] Richard G. Lugar Center for Renewable Energy, Indiana University–Purdue University, Indianapolis, IN 46202, USA
[b] Wright State University, Dayton, OH 45435, USA

HIGHLIGHTS

- We study the ethanol oxidation reaction (EOR) on Pd_xRu_y/C catalysts.
- We observe a "volcano" behavior for the EOR activity vs. the Ru atomic ratio in the Pd_xRu/C.
- The Pd_3Ru/C showed higher EOR activity than the Pd/C catalysts.
- The feasibility of AEM-DEFCs free of Pt catalyst is successfully demonstrated.

ARTICLE INFO

Article history:
Received 13 December 2012
Received in revised form
23 March 2013
Accepted 11 April 2013
Available online 9 May 2013

Keywords:
Ethanol electro-oxidation
Alkaline
PdRu/C
Anion-exchange membrane direct ethanol fuel cell

ABSTRACT

Carbon supported PdRu catalysts with various Pd:Ru atomic ratios were synthesized by impregnation method, and characterized by X-ray diffraction (XRD), transmission electron microscopy (TEM), electrochemical half-cell tests, and the anion-exchange membrane direct ethanol fuel cell (AEM-DEFC) tests. XRD results suggest that the PdRu metal exists on carbon support in an alloy form. TEM study shows that the bimetallic PdRu/C catalysts have slightly smaller average particle size than the single metal Pd/C catalyst. Lower onset potential and peak potential and much higher steady state current for ethanol oxidation in alkaline media were observed on the bimetallic catalysts (Pd_xRu_y/C) than on the Pd/C, while the activity for ethanol oxidation on the pure Ru/C was not noticeable. By using Pd/C anode catalysts and MnO_2 cathode catalysts, AEM-DEFCs free from the expensive Pt catalyst were assembled. The AEM DEFC using the bimetallic Pd_3Ru/C anode catalyst showed a peak power density as high as 176 mW cm^{-2} at 80 °C, about 1.8 times higher than that using the single metal Pd/C catalyst. The role of Ru for enhancing the EOR activity of Pd/C catalysts is discussed.

1. Introduction

With the recent advancement in anion-exchange membrane materials [1,2], there has been a growing interest in anion-exchange membrane direct alcohol fuel cell (AEM-DAFCs) technology. Compared with proton exchange membrane (PEM) based DAFCs working under acidic environment, the most significant advantages of AEM-DAFCs are [3–5]: (1) improved kinetic of both anodic alcohol oxidation reactions (AORs) and cathodic oxygen reduction reactions (ORRs), and (2) a wide range of catalyst materials besides Pt are stable in alkaline media. Consequently, AEM-DAFCs free of the expensive Pt catalyst could be developed.

Ethanol becomes an attractive fuel for AEM-DAFC applications because of its relatively high energy density and its biomass origin [6,7]. In recent years there has been much efforts going into the development of highly active anode catalyst for anion-exchange membrane direct ethanol fuel cell (AEM-DEFC), and a variety of catalyst materials, including Pt [6–9], Pd [9–15], Rh [15], Ru [16], Au [9,17,18], Ni [9,19], etc., have been tested for ethanol oxidation reaction (EOR) in alkaline media. However, among the recently reported results, only the Pt based [6–9] and Pd based [9–15] catalysts showed promising activity in the potential range practical for fuel cell application. Pd is much cheaper and more abundant than Pt. Moreover, it has been reported that Pd showed higher activity and stability for EOR than Pt in alkaline media [4,5,20]. Since the oxidation of ethanol in alkaline media is very complicated and involves many types of intermediates, such as C_1 species (most likely CO_{ad} and $CH_{x,ad}$), OH_{ad}, CH_3CO_{ad} and other forms of acetaldehyde in alkaline media [18,20,21], single metal catalysts may not

* Corresponding author. Tel.: +1 317 274 4280; fax: +1 317 274 0789.
E-mail address: rochen@iupui.edu (R. Chen).

0378-7753/$ – see front matter © 2013 Elsevier B.V. All rights reserved.
http://dx.doi.org/10.1016/j.jpowsour.2013.04.051

give the best performance for ethanol oxidation. Therefore, to further improve the activity and stability of the catalysts, substantial efforts have been devoted to modifying the Pd catalyst with a second metal M (M = Ru, Ni, Au, Sn, Ag, Cu, etc.) [10–14]. Chen et al. [10] found that the incorporation of Ru into the Pd catalyst improved the EOR activity significantly. Shen et al. [11] showed that the Pd_2Ni_3/C catalyst exhibited higher activity and stability for EOR than the Pd/C catalyst. He et al. [12] found that while the synthesized PdAu/C and PdSn/C catalyst showed inferior performance for EOR than Pt/C in the potentiodynamic test, the same catalysts showed much better performance in the potentiostatic test. Improved EOR activities have also been observed with bimetallic catalysts obtained by alloying Pd with Ag [13] and Cu [14].

It is well known that Ru promotes the alcohol electro-oxidation on Pt catalyst in acidic media. In alkaline media, Tarasevich [16] reported that RuNi catalysts (Ru atomic ratio larger than 20%) showed high activity toward EOR in the potential range practical for fuel cell application, and Kim and Park [19] found that Ru in RuNi catalyst enhanced the EOR on Ni significantly. In a preliminary study, Chen et al. [10] showed that the incorporation of Ru into the Pd catalyst improved the alcohol (methanol, ethanol and ethylene glycol) oxidation kinetics in alkaline media. However, it was noticed that the particle sizes of Pd/C (ca. 10 nm) were much larger than those of PdRu/C (too small to be calculated by XRD results) in their report. As important structural parameters in electrocatalysis studies, particle size may influences the EOR specific activity significantly.

In this study, Pd/C and Pd_xRu_y/C catalysts with similar particle sizes were prepared by an impregnation method. Cyclic voltammetry and chronoamperometry measurements demonstrated that the Pd_xRu_y/C catalysts possess higher activities toward EOR in alkaline media than the Pd/C catalyst. An AEM-DEFC using Pd_3Ru/C as the anode catalyst showed much better performance than that using Pd/C as the anode catalyst.

2. Experimental

The Pd/C, Ru/C and Pd_xRu_y/C (with various Pd:Ru atomic ratios) catalysts with 20 wt% metal loading were prepared by an impregnation method [22]. Below we describe the preparation process using the Pd_xRu_y/C catalyst as an example. The appropriate amount of $PdCl_2$ and $RuCl_3$ solutions were mixed with Vulcan XC 72 support suspension, and the mixture was heated to 80 °C with vigorous stirring under Ar gas protection. Sodium citrate solution was added to act as protective agent. Then the pH of the solution was adjusted to above 12 by gradually adding NaOH solution to the mixture. An excess of $NaBH_4$ solution was added dropwise to reduce the precursor. The suspension was then filtered and washed with excess hot ultrapure water until no Cl^- was detected. Finally, the resulting catalysts were dried at 80 °C overnight in a vacuum oven.

Transmission electron microscopy (TEM) measurements of the catalysts were carried out using a Tecnai G2 TWIN/BioTWIN microscope (FEI Company) operated at 80 kV. The X-ray diffraction (XRD) patterns of the catalysts were recorded with a Siemens X-ray diffractometer using Cu Kα radiation with a Ni filter. The tube current was 30 mA with a tube voltage of 50 kV. The 2θ angular regions between 10 and 90° were explored at a scan rate of 4° min^{-1}. The peaks of Pd (220) were used to calculate the average crystallite sizes by employing the Scherrer equation [22].

All the electrochemical measurements were conducted on a Solartron 1287 potentiostat using a standard three-electrode cell. A gold foil and a Hg/HgO/NaOH (1.0 M NaOH) electrode served as the counter and reference electrodes, respectively. However, all the potentials reported in this study refer to the reversible hydrogen electrode (RHE). The catalyst suspension was prepared according to the procedure described in a previous report by the present authors [20]. Prior to the electrochemical tests, the prepared thin film electrodes were first cycled between 0.06 and 1.2 V in an Ar-saturated blank NaOH solution. For chronoamperometry (CA) measurements, after the electrode was held at a potential of 0.09 V for 50 s to obtain a baseline, the electrode was stepped to the potentials between 0.45 and 0.55 V in 0.05 V increments. Each data set was recorded with a single electrode, i.e. after stepping from 0.09 to 0.45 V, a further step to the following potential was performed [20]. All the potentials were IR corrected by Solartron operation software.

The fuel cell performance test was performed using a single cell with an active area of 4.5 cm^2. The membrane electrode assemblies (MEAs) were comprised of a catalyst coated membrane (CCM), a Ni foam (Hohsen Corp.) as the anode backing layer and a TGP-H-090 carbon paper (Toray) as the cathode backing layer. The CCM was fabricated by direct spraying the catalyst ink onto an A201 membrane (Tokuyama Co.). The anode catalyst ink was prepared by mixing the catalyst (20 wt% Pd/C or 20 wt% Pd_3Ru/C) and a 5 wt% Nafion binder with ethanol. The cathode catalyst ink was prepared by ultrasonicating the MnO_2 nanotube catalyst produced in our lab [23], active carbon (BP2000, Cabot Corp.), and the A4 ionomer (Tokuyama Co.) with a THF/methanol mixed solvent. The anode catalyst loading was 10 mg cm^{-2} (noble metal loading was 2 mg cm^{-2}), while the cathode catalyst loading was 2 mg cm^{-2}. The MEA was sandwiched between two graphite bipolar plates. The fuel cell tests were conducted on a Scribner Associates Model 850e test station. The liquid fuel (3 M ethanol + 3 M KOH solution) was pumped to the anode at a rate of 2 ml min^{-1} and dried oxygen gas (Praxair Inc.) was fed to the cathode at 300 sccm. The temperature of the fuel cell was maintained with a tolerance of ±0.2 °C. The polarization curves were obtained by measuring the cell voltage at different currents after reaching steady state.

3. Results and discussion

XRD patterns of the Ru/C, Pd_xRu_y/C (with Pd:Ru atomic ratio of 1:1, 2:1, 3:1 and 4:1) and Pd/C catalysts are given in Fig. 1. All the catalysts showed a broad peak located around 25° corresponding to the (002) plane of the Vulcan XC 72 carbon support. In addition to the diffraction peak of carbon, the Ru/C catalyst showed a single broad peak located around 44°, indicating that Ru was dispersed on carbon support either in a very small nanoparticle size or in an amorphous state [15]. While the Pd/C catalyst showed four more peaks located around 40°, 47°, 68°, and 82°, which were attributed to the (111), (200), (220), and (311) plane of the Pd face-centered cubic (fcc) structure. All the Pd_xRu_y/C catalysts showed an fcc structure similar to that of the Pd/C catalyst. When the Ru content was high, as shown in the XRD of the PdRu/C (Pd:Ru = 1:1) catalyst, the peaks of the (111) and (200) planes were merged into a single broad peak, while the peaks of the (220) and (311) planes became weak and broad. Comparing with Pd/C, the diffraction peaks of all the Pd_xRu_y/C shifted slightly to the higher 2θ values (e.g. the (220) peak was located at 67.9°, 68.3°, 68.4° and 68.5° for the Pd/C, Pd_4Ru/C, Pd_3Ru/C and Pd_2Ru/C, respectively.). The lattice constants were calculated using the Pd (220) peak and values are found to be 0.3901, 0.3881, 0.3876 and 0.3871 nm for the Pd/C, Pd_4Ru/C, Pd_3Ru/C and Pd_2Ru/C catalyst, respectively [22]. The decrease of the lattice constant with increasing Ru concentration in PdRu bimetallic catalyst indicates that PdRu alloy was formed [24].

The average crystallite size of the catalysts was calculated from the (220) peak using the Scherrer equation which avoids the interference from the diffraction of the carbon support [22] :

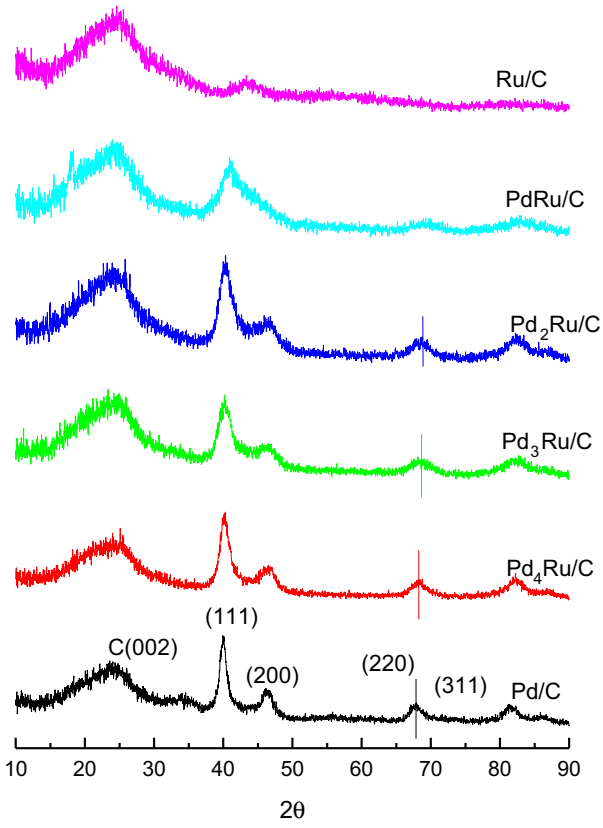

Fig. 1. X-ray diffractograms of Ru/C, PdRu/C and Pd/C electrocatalysts.

$$d = \frac{k\lambda_K}{B_{2\theta}\cos\theta_{\max}}$$

where k is a coefficient (0.9), λ_K is the X-ray wavelength of Cu $K_{\alpha 1}$ radiation (=0.154056 nm), $B_{2\theta}$ is the half-peak width of the (220) peak (in radian) and $\theta_{\max}$ is the angle of the maximum peak position. The crystallite sizes of the Pd/C, Pd_4Ru/C, Pd_3Ru/C and Pd_2Ru/C were estimated from the XRD results to be 3.4 nm, 3.1 nm, 2.9 nm and 3.0 nm, respectively.

The typical TEM images and corresponding particle size distributions of the Ru/C, Pd_3Ru/C and Pd/C catalysts are shown in Fig. 2. Consistent with the XRD results, no discernible particles were found in the TEM image of the Ru/C (Fig. 2a). From the TEM images of the Pd_3Ru/C (Fig. 2b) and Pd/C (Fig. 2c), it can be seen that all the nanoparticles were dispersed on the carbon support uniformly. The histograms for particle size distribution of the Pd_3Ru/C (Fig. 2d) and Pd/C (Fig. 2e) were obtained by measuring the sizes of 100 randomly selected particles in the TEM images. The particle sizes of the Pd/C catalyst range from 2.2 nm to 5.2 nm, with an average particle size of 3.4 nm. The Pd_3Ru/C catalyst has a particle size distribution ranging from 1.5 to 4.4 nm. The average particle size of Pd_3Ru/C is 2.8 nm, slightly smaller than that of the Pd/C.

Fig. 3 shows the cyclic voltammograms (CVs) of the Ru/C, Pd_3Ru/C and Pd/C catalysts in an Ar-saturated 1 M NaOH solution. The Pd/C catalyst produced a typical CV profile in the alkaline media, in which the adsorption of OH started immediately after desorption of hydrogen, and gave rise to a small peak located around 0.49 V [20,25]. The Ru/C result shows a pair of broad peak in the potential range of 0.2–0.8 V, which is the characteristic of RuO_xH_y formation [26,27]. At high potentials ($E > 0.9$ V), the oxidation current resurged, corresponding to the formation of bulk RuO_2 or high valence Ru oxides [26,27]. For the Pd_3Ru/C catalyst, the hydrogen adsorption/desorption region and the oxides formation/reduction of the Pd species overlapped with the redox of the RuO_xH_y species, giving an ill-resolved broad peak in the potential region below 0.8 V, which is much like a pseudo-capacitor behavior. This indicates that not all the Ru species in the Pd_3Ru/C catalyst existed in alloy form, at least some of the Ru presented in an amorphous form.

The CVs of ethanol oxidation in Ar-saturated 1 M NaOH + 1 M ethanol solution on the Pd/C and Pd_xRu_y/C catalysts are shown in Fig. 4. All the currents are normalized to the mass of the noble metal (mA per mg of noble metal) for comparison. The Pd/C CV shows an oxidation peak located around 0.9 V in the positive scan and a sharp peak located around 0.76 V in the negative scan, which is the typical CV shape for ethanol oxidation [20]. For all the Pd_xRu_y/C catalyst tested, an oxidation peak in the positive scan and two peaks (a sharp peak located at the higher potential region and another broad peak located at the lower potential region) in the negative scan can be observed. Moreover, the ratio between the peak current in the forward scan (i_f) and that in the backward scan (i_b) is lower than that for Pd/C. This indicates that the Pd surface is more severely poisoned by adsorbed intermediates on the Pd_xRu_y/C catalysts than on the Pd/C catalyst. These characteristics are different from what was previously reported on PdM (M = Ni, Au, Sn, Ag, Rh) catalysts [11–13,15]. In those reports, all the catalysts had similar CV patterns for ethanol oxidation as that of the Pd/C catalyst. The different CV patterns of Pd_xRu_y/C indicate that the ethanol oxidation pathway has changed on these catalysts. It is known that ethanol oxidation in alkaline media goes through a dual-path mechanism [20,21]. In the C_2 pathway, partially oxidation products such as acetaldehyde and acetate are produced due to the difficulty in breaking the C–C bond. In the C_1 pathway, the C–C bonds break down and generate the strongly adsorbed C_1 species (CO_{ad} and $CH_{x,ad}$). Zhou et al. [28] reported that the selectivity for ethanol oxidation to carbonate in alkaline media on Pd electrode was as low as 2.5% using FTIR. Therefore, the main ethanol oxidation pathway on Pd/C would be the C_2 pathway [20,28]. On Pd_xRu_y/C catalyst, besides the C_2 pathway, more complicated ethanol oxidation pathways exist.

To better understand the origins of the differences in CV patterns, the ethanol oxidation behavior on Ru/C catalyst is given in Fig. 5a. For potentials lower than 0.8 V, a similar pseudo-capacitor behavior was observed for Ru/C in the Ar-saturated 1 M NaOH + 1 M ethanol solution as that in the blank 1 M NaOH solution. EOR current is only noticeable for potentials high than 0.9 V, which corresponds to the formation of high valence Ru oxides. Clearly, Ru/C is inactive for ethanol oxidation in the potential range practical for fuel cell. However, the Pd_xRu_y/C catalyst showed a much lower onset potential (e. g. 0.2 V for Pd_3Ru/C) for EOR, as shown in the Fig. 5b. Therefore, the change of ethanol oxidation pathway on the Pd_xRu_y/C catalyst should not be solely attributed to the Ru species; the synergistic effects between the Pd species and Ru species apparently play an important role. All the Pd_xRu_y/C catalysts produced lower onset potential and peak potential for EOR than the Pd/C, as shown in the insert of Fig. 4. The Pd_xRu_y/C catalysts generated lower peak currents during the positive scans at the higher potential range, but higher currents during both the positive scans and the negative scans at the lower potential range. Chen et al. [10] also reported the lower onset potential and higher oxidation current for EOR at lower potentials for the PdRu/C catalyst as compared to the Pd/C from their linear sweep voltammetry (LSV) tests. These results indicate that the bimetallic Pd_xRu_y/C catalysts are more active than the single metal Pd/C catalyst for AEM-DEFC applications.

The quasi-steady state currents for ethanol oxidation on the Pd/C and Pd_xRu_y/C catalysts measured by chronoamperometry (CA) are

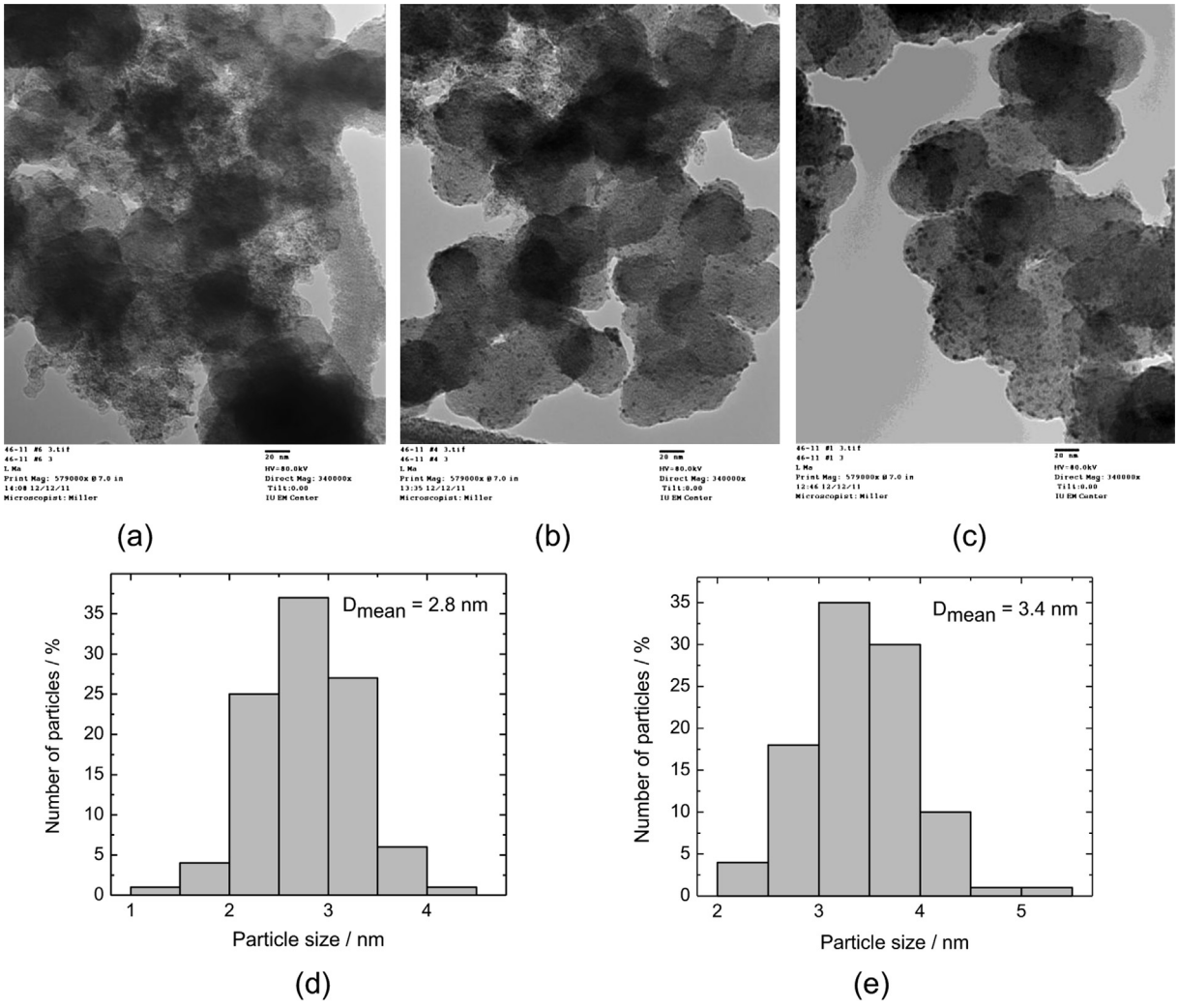

Fig. 2. TEM images of (a) Ru/C, (b) Pd_3Ru/C and (c) Pd/C and the corresponding particle distributions of (d) Pd_3Ru/C and (e) Pd/C.

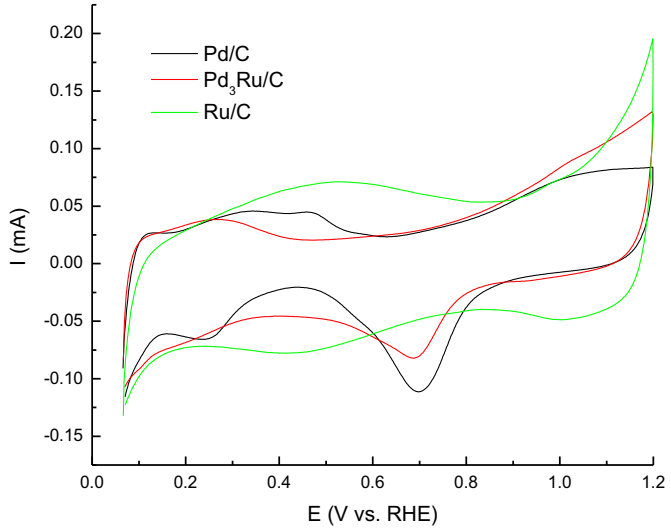

Fig. 3. The CVs of Ru/C, Pd_3Ru/C and Pd/C electrocatalysts in an Ar-saturated 1 M NaOH solution. Scanning rate: 10 mV s^{-1}.

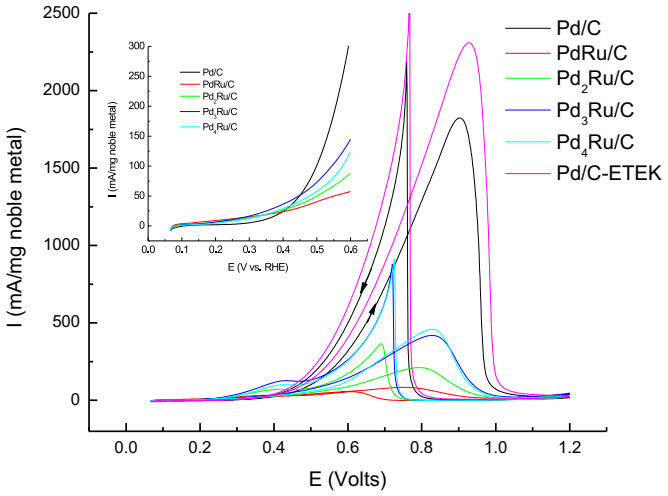

Fig. 4. The CVs of Ru/C, PdRu/C, Pd/C and commercial Pd/C-ETEK electrocatalysts in an Ar-saturated 1 M NaOH + 1 M ethanol solution (insert: enlarged CVs). Scanning rate: 10 mV s^{-1}.

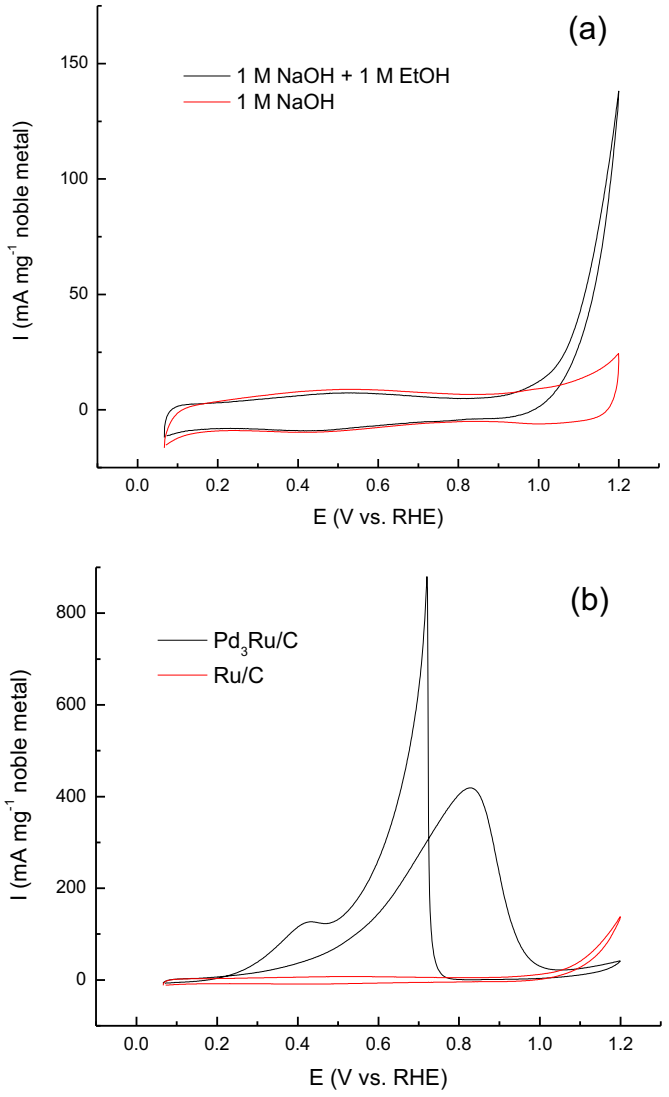

Fig. 5. The electrochemical behavior of (a) Ru/C in 1 M NaOH solution and 1 M NaOH + 1 M ethanol solutions; (b) Ru/C vs. Pd_3Ru/C in 1 M NaOH + 1 M ethanol solution. Scanning rate: 10 mV s^{-1}.

shown in Fig. 6. The quasi-steady state currents were recorded after 15 min of polarization at each potential. The Faradaic currents of the Pd/C decayed slowly with time. On all the Pd_xRu_y/C catalysts, however, the Faradaic currents increased at first, giving rise to a current spike, and then decayed slowly with time. This current spike was more pronounced at high potentials. The following factors could potentially contribute to the current spike [8]: (1) instantaneous oxidation of hydrogen adlayer, (2) simultaneous dissociative adsorption of ethanol, (3) pseudocapacitive currents (mostly come from Ru, as shown in Fig. 4b). The accumulation of strongly adsorbed species (adsorbed CO_{ad} and hydrocarbon residues) due to dissociative ethanol on Pd_xRu_y/C is primarily responsible for the gradual decay of currents [8]. At 0.45 V, all of the Pd_xRu_y/C catalysts produced higher steady currents for EOR than the Pd/C catalyst with the order of performance following $Pd_3Ru/C > PdRu/C > Pd_2Ru/C > Pd_4Ru/C$. As the polarization potential increases, the steady current increases correspondingly for all the catalysts. However, the Pd_xRu_y/C catalysts with high Ru content responded slower to potential changes; in fact, at 0.55 V, the steady currents of PdRu/C and Pd_2Ru/C are lower than that of Pd/C. As shown in Fig. 7, the steady current for EOR shows 'volcano' behavior

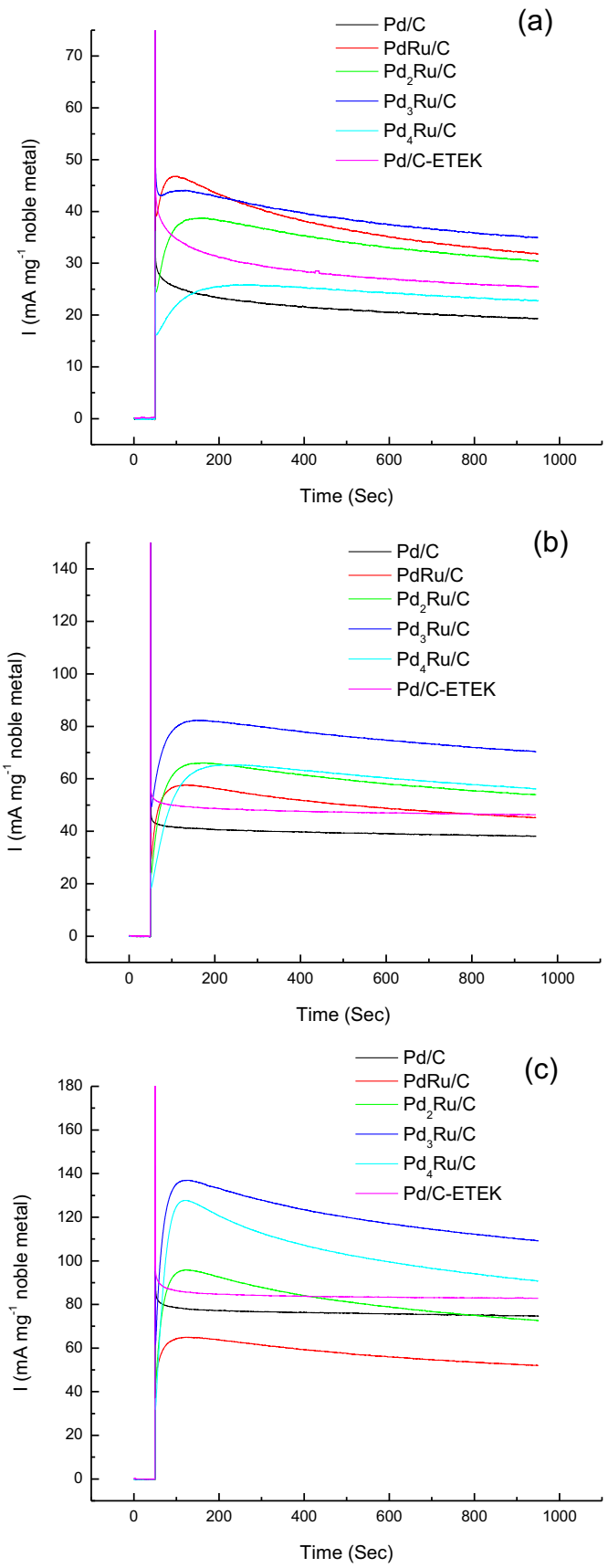

Fig. 6. The CAs of electrodes in an Ar-saturated 1 M NaOH + 1 M ethanol solution at potential of (a) 0.45 V, (b) 0.5 V and (c) 0.55 V.

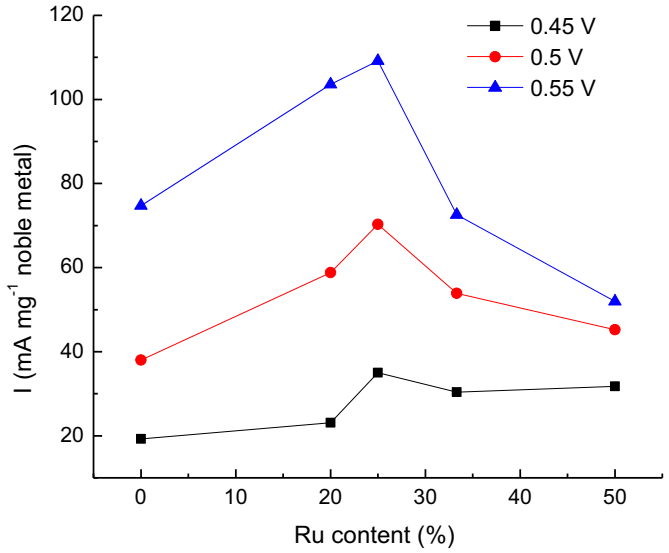

Fig. 7. Dependence of the EOR activity of the Pd_xRu_y/C catalyst on the Ru atomic ratio.

as a function of the Ru atomic ratio in the Pd_xRu_y/C catalyst, in which the EOR activity of the Pd_xRu_y/C increases with the increasing of the Ru content from 0 to 25% (i.e. Pd:Ru atomic ratio of 3:1) and decreases further with the increasing of Ru content to 100% (i.e. Ru/C). The highest steady current is gotten on the Pd_3Ru/C catalyst at all the potentials, which is about 1.5 to 1.8 times higher than that of the Pd/C catalyst.

It is interesting to note that the Pd_3Ru/C catalyst showed lower onset potential in the CV test and higher steady current in the CA tests than the Pd/C. In comparison with the Pd/C, the Pd_3Ru/C catalyst showed dual-peak characteristic in the negative scan and higher current at the lower potentials. Also, the ratio between the peak current in the forward scan (i_f) and that in the backward scan (i_b) is lower. These characteristics indicate that the ethanol oxidation pathway on the Pd_3Ru/C catalyst was different from that on Pd/C catalyst. For Pd/C catalyst, the ethanol oxidation mainly goes through the C_2 pathway [20,21,28]. From the FTIR study of Pd catalyst, a weak band assigned to bridge-bonded CO ($CO_{B,\ ad}$) was also found [28]. This confirmed that there is strongly adsorbed CO species on Pd electrode during the ethanol oxidation. However, the Pd−CO_{ad} is so strong that the CO_{ad} species are hard to be removed through oxidation, as evidence by the high CO stripping potential of Pd electrode [24]. This may also contribute to the low selectivity of ethanol oxidation to carbonate in alkaline media determined by FTIR. For Pd_xRu_y/C catalysts, the ethanol oxidation pathway is more complex as evidenced by the significant changes in CV profiles. Recently, Behm's group [29] found that compared to a pure Pd(111) surface, the CO adsorption on the Pd sites of the PdRu/Ru(0001) surface or Pd monolayer on Ru(0001) are significantly weaker due to the combination of geometric strain and vertical electronic ligand effects. Fisher et al. [24] also found the CO stripping peak on PdRu/C was to be much lower than that on Pd/C in acidic media. Therefore, it is reasonable to infer that the oxidation removal of CO species would be much easier on the Pd_xRu_y/C catalyst, and the C_1 pathway would be promoted, which is also demonstrated by the two oxidation peaks present in the backward scan on the Pd_xRu_y/C catalysts. We propose the following explanation to the enhancement of EOR on Pd_3Ru/C: (1) Similar to the enhancement of methanol oxidation on PtRu/C catalysts in acidic media [22,26], the formation of RuO_xH_y at low potentials (Fig. 3) facilitates the ethanol oxidation on Pd_3Ru/C. (2) The CO adsorption on Pd_3Ru/C is weaker and thus the oxidation removal of the adsorbed CO is easier. Both these effects would contribute to the significant enhancement of EOR on Pd_3Ru/C.

Fig. 8 shows the polarization and the corresponding power density curves of the AEM-DEFCs using the Pd_3Ru/C and the Pd/C catalysts at the anodes. For all the tested temperatures, the open-circuit voltage (OCV) of the AEM DEFC using the Pd_3Ru/C anode

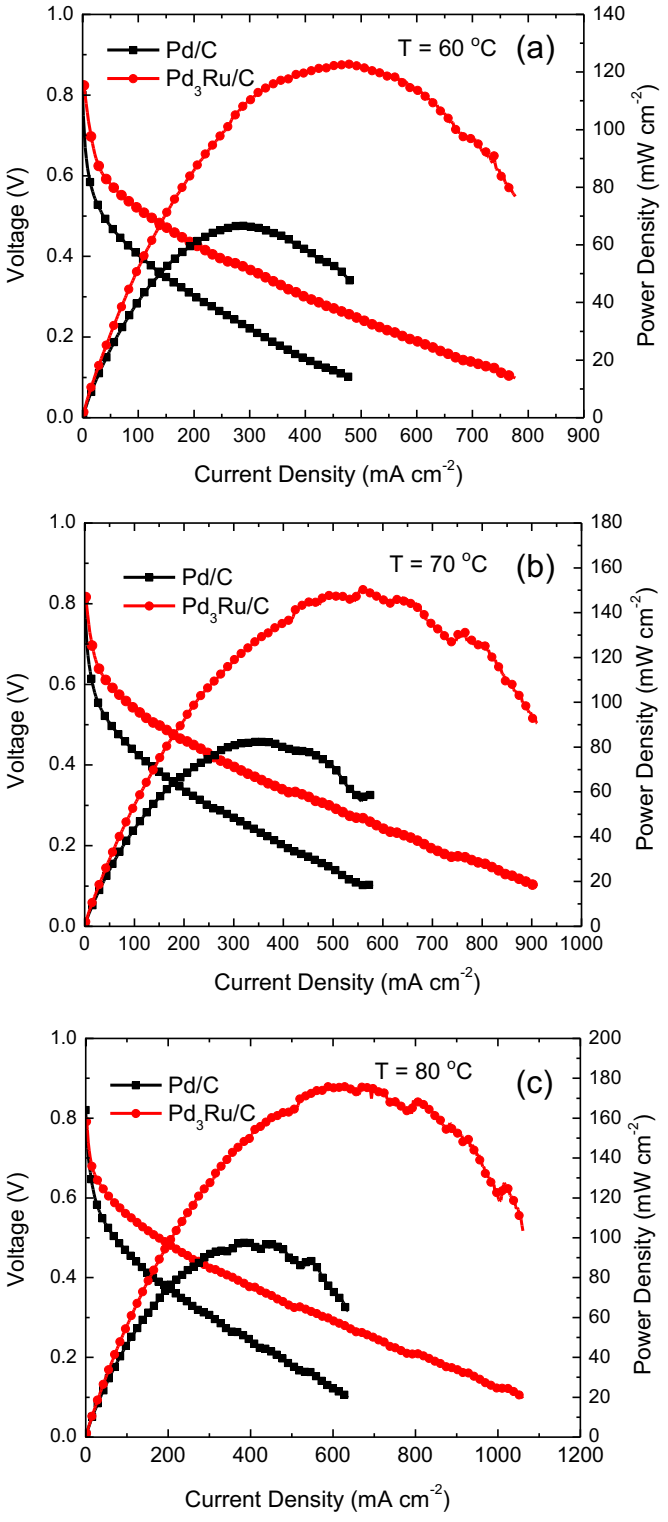

Fig. 8. Polarization and power density curves of the AEM DEFC using various anode catalysts at different temperature (a) 60 °C, (b) 70 °C and (c) 80 °C.

catalyst is higher than that using the Pd/C anode catalyst. For example, at 60 °C, the OCV of the AEM-DEFC using Pd_3Ru/C was 0.82 V as compared to 0.75 V for the cell using the Pd/C anode catalyst. The peak power densities of the AEM DEFC using Pd_3Ru/C are 123 mW cm^{-2}, 151 mW cm^{-2} and 176 mW cm^{-2} at 60 °C, 70 °C and 80 °C, respectively. While the peak power density of the AEM DEFC using Pd/C is 67 mW cm^{-2}, 82 mW cm^{-2} and 98 mW cm^{-2} for 60 °C, 70 °C and 80 °C, respectively. For all the temperatures tested, the performance of the fuel cell using Pd_3Ru/C was about 1.8–2 times higher than that using Pd/C.

4. Conclusions

Pd_xRu_y/C catalysts were synthesized and characterized for ethanol oxidation in both electrochemical half-cell and AEM-DEFC tests. The prepared Pd_xRu_y/C catalysts showed slightly smaller average particle size than the Pd/C. XRD indicated that PdRu existed on carbon support in the form of alloy. The EOR activity of Pd_xRu_y/C catalyst showed 'volcano' behavior as a function of the Ru atomic ratio in the Pd_xRu_y/C, in which the highest activity was gotten on the Pd_3Ru/C catalyst. The Pd_3Ru/C catalyst showed much higher activity toward EOR than the Pd/C catalyst in the practical fuel cell potential range, as shown in both the CV and CA tests. The feasibility of AEM-DEFCs free of Pt catalyst is successfully demonstrated. The AEM DEFC using the Pd_3Ru/C as anode catalyst showed a peak power density as high as 176 mW cm^{-2} at 80 °C, about 1.8 times higher than that using Pd/C as anode catalyst. The enhancement of EOR on the Pd_3Ru/C is attributed to: (1) the formation of RuO_xH_y at low potentials, and (2) weakened CO adsorption on Pd_3Ru/C.

Acknowledgments

This work was partially supported by the U.S. Army Research Office.

References

[1] J.R. Varcoe, R.C.R. Slade, Fuel Cells 5 (2005) 187–200.
[2] J. Pan, C. Chen, L. Zhuang, J. Lu, Acc. Chem. Res. 45 (2011) 473–481.
[3] Y. Wang, L. Li, L. Hu, L. Zhuang, J. Lu, B. Xu, Electrochem. Commun. 5 (2003) 662–666.
[4] C. Bianchini, P.K. Shen, Chem. Rev. 109 (2009) 4183–4206.
[5] E. Antolini, E.R. Gonzalez, J. Power Sources 195 (2010) 3431–3450.
[6] M.M. Tusi, N.S.O. Polanco, S.G. da Silva, E.V. Spinacé, A.O. Neto, Electrochem. Commun. 13 (2011) 143–146.
[7] S.Y. Shen, T.S. Zhao, J.B. Xu, Int. J. Hydrogen Energy 35 (2010) 12911–12917.
[8] L. Jiang, A. Hsu, D. Chu, R. Chen, Int. J. Hydrogen Energy 35 (2010) 365–372.
[9] D. Bayer, C. Cremers, H. Baltruschat, J. Tubke, ECS Trans. 41 (2011) 1669–1680.
[10] Y. Chen, L. Zhuang, J. Lu, Chin. J. Catal. 28 (2007) 870–874.
[11] S.Y. Shen, T.S. Zhao, J.B. Xu, Y.S. Li, J. Power Sources 195 (2010) 1001–1006.
[12] Q. He, W. Chen, S. Mukerjee, S. Chen, F. Laufek, J. Power Sources 187 (2009) 298–304.
[13] G. Li, L. Jiang, Q. Jiang, S. Wang, G. Sun, Electrochim. Acta 56 (2011) 7703–7711.
[14] W.-D. Kang, Y.-C. Wei, C.-W. Liu, K.-W. Wang, Electrochem. Commun. 13 (2011) 162–165.
[15] Y. Suo, I.M. Hsing, J. Power Sources 196 (2011) 7945–7950.
[16] M.R. Tarasevich, Z.R. Karichev, V.A. Bogdanovskaya, E.N. Lubnin, A.V. Kapustin, Electrochem. Commun. 7 (2005) 141–146.
[17] G. Tremiliosi-Filho, E.R. Gonzalez, A.J. Metheo, E.M. Belgsir, J.M. Leger, C. Lamy, J. Electroanal. Chem. 444 (1998) 31–39.
[18] Y. Kwon, S.C.S. Lai, P. Rodriguez, M.T.M. Koper, J. Am. Chem. Soc. 133 (2011) 6914–6917.
[19] J.-W. Kim, S.-M. Park, J. Electrochem. Soc. 150 (2003) E560–E566.
[20] L. Ma, D. Chu, R. Chen, Int. J. Hydrogen Energy 37 (2012) 11185–11194.
[21] S.C.S. Lai, S.E.F. Kleijn, F.T.Z. Ozturk, V.C. van Rees Vellinga, J. Koning, P. Rodriguez, M.T.M. Koper, Catal. Today 154 (2010) 92–104.
[22] L. Ma, C. Liu, J. Liao, T. Lu, W. Xing, J. Zhang, Electrochim. Acta 54 (2009) 7274–7279.
[23] W. Sun, A. Hsu, R. Chen, J. Power Sources 196 (2011) 4491–4498.
[24] J.M. Fisher, N. Cabello-Moreno, E. Christian, D. Thompsett, Electrochem. Solid-State Lett. 12 (2009) B77–B81.
[25] L.D. Burke, J.K. Casey, J. Electrochem. Soc. 140 (1993) 1292–1298.
[26] H.A. Gasteiger, N. Markovic, P.N. Ross, E.J. Cairns, J. Phys. Chem. 97 (1993) 12020–12029.
[27] P. Kurzweil, J. Power Sources 190 (2009) 189–200.
[28] Z.-Y. Zhou, Q. Wang, J.-L. Lin, N. Tian, S.-G. Sun, Electrochim. Acta 55 (2010) 7995–7999.
[29] H. Hartmann, T. Diemant, J. Bansmann, R.J. Behm, Surf. Sci. 603 (2009) 1456–1466.